NASA/TP—2016–219072

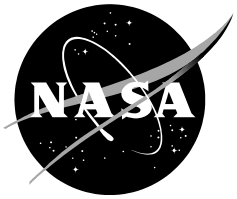

On Wings of the Minimum Induced Drag: Spanload Implications for Aircraft and Birds

Albion H. Bowers, and Oscar J. Murillo
Armstrong Flight Research Center, Edwards, California

Robert "Red" Jensen, and Brian Eslinger
Jacobs Technology, Inc., Edwards, California

Christian Gelzer
Logical Innovations, Inc., Edwards, California

March 2016

NASA STI Program ... in Profile

Since its founding, NASA has been dedicated to the advancement of aeronautics and space science. The NASA scientific and technical information (STI) program plays a key part in helping NASA maintain this important role.

The NASA STI program operates under the auspices of the Agency Chief Information Officer. It collects, organizes, provides for archiving, and disseminates NASA's STI. The NASA STI program provides access to the NTRS Registered and its public interface, the NASA Technical Reports Server, thus providing one of the largest collections of aeronautical and space science STI in the world. Results are published in both non-NASA channels and by NASA in the NASA STI Report Series, which includes the following report types:

- TECHNICAL PUBLICATION. Reports of completed research or a major significant phase of research that present the results of NASA Programs and include extensive data or theoretical analysis. Includes compilations of significant scientific and technical data and information deemed to be of continuing reference value. NASA counterpart of peer-reviewed formal professional papers but has less stringent limitations on manuscript length and extent of graphic presentations.

- TECHNICAL MEMORANDUM. Scientific and technical findings that are preliminary or of specialized interest, e.g., quick release reports, working papers, and bibliographies that contain minimal annotation. Does not contain extensive analysis.

- CONTRACTOR REPORT. Scientific and technical findings by NASA-sponsored contractors and grantees.

- CONFERENCE PUBLICATION. Collected papers from scientific and technical conferences, symposia, seminars, or other meetings sponsored or co-sponsored by NASA.

- SPECIAL PUBLICATION. Scientific, technical, or historical information from NASA programs, projects, and missions, often concerned with subjects having substantial public interest.

- TECHNICAL TRANSLATION. English-language translations of foreign scientific and technical material pertinent to NASA's mission.

Specialized services also include organizing and publishing research results, distributing specialized research announcements and feeds, providing information desk and personal search support, and enabling data exchange services.

For more information about the NASA STI program, see the following:

- Access the NASA STI program home page at http://www.sti.nasa.gov

- E-mail your question to help@sti.nasa.gov

- Phone the NASA STI Information Desk at 757-864-9658

- Write to:
  NASA STI Information Desk
  Mail Stop 148
  NASA Langley Research Center
  Hampton, VA 23681-2199

NASA/TP—2016–219072

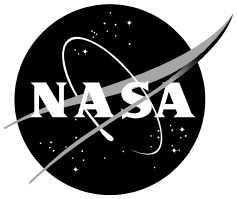

On Wings of the Minimum Induced Drag: Spanload Implications for Aircraft and Birds

Albion H. Bowers, and Oscar J. Murillo
Armstrong Flight Research Center, Edwards, California

Robert "Red" Jensen, and Brian Eslinger
Jacobs Technology, Inc., Edwards, California

Christian Gelzer
Logical Innovations, Inc., Edwards, California

National Aeronautics and
Space Administration

Armstrong Flight Research Center
Edwards, California, 93523-0273

March 2016

Acknowledgments

Many people contributed directly to this work through their ideas, comments, suggestions, and assistance. The authors concede that many people are likely inadvertently omitted from the list below, and we express our apologies for any collective failures of memory. Our thanks to: Derek Abramson, Keenan Albee, Sipanah Arutyunyan, Chris Acuff, Mike Agnew, Mike Allen, Luis Andrade, Dan Banks, Leo Banuelos, Sam Batarseh, Nathan Bell, Dave Berger, Olivia Bosma, Jason Bowen, Jerry Budd, Michael Butros, Andrew Burrell, Dennis Calaba, Kimmie Calahan, Alex Chen, Paul Dees, John Del Frate, Bryce Doerr, Louis Edelman, Ana Escalera, Cynthia Farr, David Faust, Kirsten Fogg, Mike Frederick, Katherine Glasheen, Scott Gleason, Jacob Gustafson, Eric Gutierrez, Jacob Hall, Adam Harding, Etan Halberg, Ross Hathaway, Bob Hoey, Sanel Horozovic, Reimar Horten, Walter Horten, Richard M. Howard, Taylor Jensen, Kristyn Kadala, Cody Karcher, Mike Kerho, Kurt Kloesel, David Kloesel, Michael Kloesel, Brian Kramer, Elizabeth Kissling, Heather Laffoon, Cameron Law, David Lee, Russell Lee, Jack Levine, Mandy Ledford, Jay Levine, Caleb Lloyd, Victor Loera, Arlene Lopez, Joe Lorenzetti, Kyle Lukacovic, Justine Mack, Paul MacCready, Anthony MacPherson, Kassidy McLaughlin, Mike Marston, Orlando Mielke, Chris Miller, Matt Moholt, Rick Motalwakel, Lesli Monforton, William Morris, Jim Murray, Hussein Nasr, Golda Nguyen, Gunhilde Horten Nickel, Karl Nickel, Eric Nisbet, Alexandra Ocasio, Joe Pahle, Steve Parcel, Kurt Pauer, Nancy Pinon, Joseph Piotrowski, Brian Plank, Bogdan Pugach, Andy Putch, Ronalynn Ramos, Nalin Ratnayake, Chris Regan, Nickelle Reid, Stephanie Reynolds, Rebecca Richardson, Jeromy Robbins, Javier Rocha, Emma Ruano, Victor Ruiz, Aamod Samuel, Peter Selinger, Jaiwon Shin, Alec Sim, Patrick Soza, Amada Spakes, Reinhold Stadler, Marko Stamenovic, Alex Stuber, Curtis Stump, Ed Swan, Josh Tanon, Brian Taylor, Jack Toth, Tom Tschida, Edward Uden, Julianna Plumb Ulrich, Eduardo Uribe-Saldana, Christos Valiotis, Moiz Vahora, Lynn Valkov, Steffi Valkov, Koen vander Kerckhove, David Voracek, Joey Wagster, Kaixi Wang, Shelby Worrell, Hovig Yaralian, Seung “Paul” Yoo, and Jonathan Zur.

NASA STI Support Services
Mail Stop 148
NASA Langley Research Center
Hampton, VA 23681-2199
757-864-9658

National Technical Information Service
5301 Shawnee Rd.
Alexandria, VA 22312
webmail@ntis.gov
703-605-6000

Abstract

For nearly a century Ludwig Prandtl's lifting-line theory remains a standard tool for understanding and analyzing aircraft wings. The tool, said Prandtl, initially points to the elliptical spanload as the most efficient wing choice, and it, too, has become the standard in aviation.

Having no other model, avian researchers have used the elliptical spanload virtually since its introduction. Yet over the last half-century, research in bird flight has generated increasing data incongruous with the elliptical spanload.

In 1933 Prandtl published a little-known paper presenting a superior spanload: any other solution produces greater drag. We argue that this second spanload is the correct model for bird flight data. Based on research we present a unifying theory for superior efficiency and coordinated control in a single solution. Specifically, Prandtl's second spanload offers the only solution to three aspects of bird flight: how birds are able to turn and maneuver without a vertical tail; why birds fly in formation with their wingtips overlapped; and why narrow wingtips do not result in wingtip stall.

We performed research using two experimental aircraft designed in accordance with the fundamentals of Prandtl's second paper, but applying recent developments, to validate the various potentials of the new spanload, to wit: as an alternative for avian researchers, to demonstrate the concept of proverse yaw, and to offer a new method of aircraft control and efficiency.

Introduction

In 1922 Ludwig Prandtl published his "lifting line" theory in English; the tool enabled the calculation of lift and drag for a given wing. Using this tool results in the optimum spanload for minimum induced drag (the greatest efficiency) for a given span, which, Prandtl said, was elliptical (ref. 1). Since then, the lifting line theory and elliptical spanload have become the standard design tool and wing spanloading in aviation. So ubiquitous is it that avian researchers have relied on it to explain bird flight data almost since its introduction. But in 1933 Prandtl published a second paper on the subject in which he conceded that his first conclusion was incomplete: there was a superior spanload solution to maximum efficiency for a given structural weight. "That the wingspan has to be specified," he wrote, "leads to the invalid assertion that the elliptical distribution is best" (ref. 2). His new bell-shaped spanload creates a wing that is 11 percent more efficient and has 22 percent greater span than its elliptically-loaded cousin, all while using exactly the same amount of structure. It results in the minimum drag solution in every case of physical wings: any other solution will produce greater drag. Oddly, Prandtl's second spanload remains virtually unknown.

Sometime around 1935 Reimar Horten independently derived an approximate equivalent to Prandtl's 1933 solution. Horten dubbed it "bell shaped" for its wing loading. The extant evidence shows sufficient differences between the two men's methods, objectives, and conclusions to exclude any mingling of information on this subject despite being contemporaries. While Prandtl calculated the total induced drag for a wing with this new spanload, he did not examine the distribution of the induced drag across the span, and so he missed its implications. Horten, on the other hand, did calculate the induced drag across the span of the wing, and in 1950 concluded that something singularly possible existed with such a spanload, although he never conclusively proved it (refs. 3, 4). What Prandtl missed and Horten believed existed with respect to the alternate spanloading (the bell) is proverse yaw. Figure 1 shows the elliptical and bell spanloads of Ludwig Prandtl.

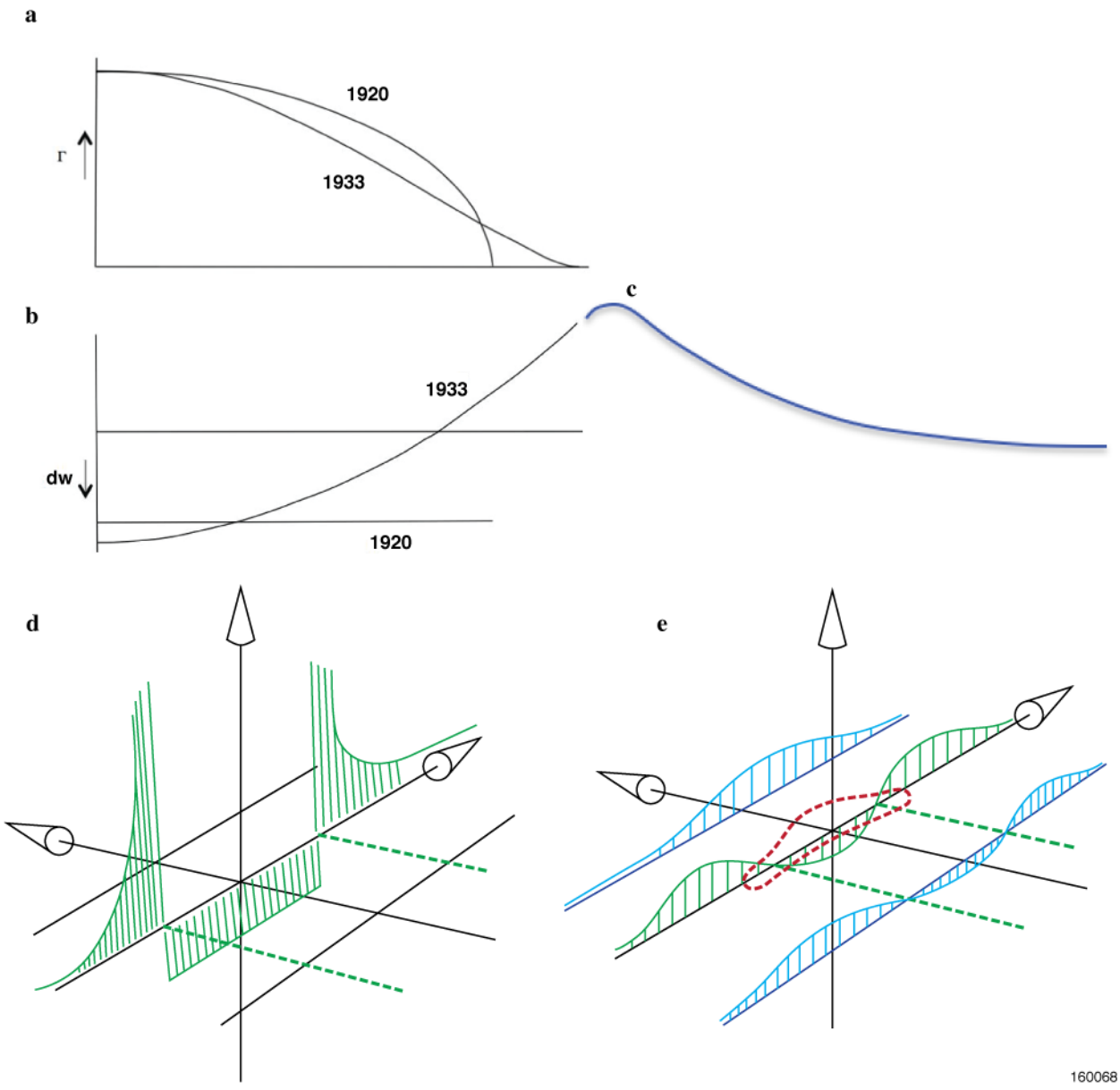

Figure 1. The elliptical and bell spanloads of Ludwig Prandtl.

Figure 1(a) shows Prandtl's elliptical spanload from 1920 and the bell spanload from 1933. The symbol gamma (Γ) signifies the airflow circulation about the wing. Figure 1(b) shows the matching downwash (dw) of the elliptical spanload (1920) and the downwash of the bell spanload (1933). In figure 1(c) the upwash outboard of the wingtip is shown. Figure 1(d) shows the 1920 Prandtl elliptical spanload downwash and upwash (note the sharp discontinuity at the wingtip, which is the wingtip vortex). Figure 1(e) shows the 1933 Prandtl spanload downwash and upwash (in contrast to the 1920 solution, note the smooth, continuous upwash across the wing and beyond; the wing vortex is now inboard of the tips). A comparison of the flow fields resulting from the elliptical and bell spanloads is shown in figures 1(d) and 1(e). The elliptical spanload wing, figure 1(d), has a sharp discontinuous slope at the wingtip span location in the upwash (this is the location of the wingtip vortex), in contrast to the smooth curve of the new upwash, figure 1(e) with no discontinuity (a weak vortex forms at the point where the downwash crosses the zero line and becomes upwash).

Prandtl's 1933 solution is stated as

$$L = (1 - x^2)^{3/2}$$

where L is the nondimensional local load (this is also expressed as gamma or Γ); and x is the span location between 0 and 1. Subsequently,

$$DW = 3/2 (x^2 - ½)$$

where DW is the nondimensional downwash (angle) of the flow.

The lift approaches zero at the wingtip, as shown in equation (1):

$$\lim_{x:\, 0 \rightarrow b/2} L(x) = 0 \qquad (1)$$

The slope of the lift (as a function of span) approaches zero at the wingtip, as shown in equation (2):

$$\lim_{x:\, 0 \rightarrow b/2} \frac{dL(x)}{dx} = 0 \qquad (2)$$

The slope of the upwash (as a function of span) at the wingtip is equal on both sides of the wingtip, as shown in equation (3):

$$\lim_{x:0 \rightarrow b/2} \frac{d\,DW(x)}{dx} = \lim_{x:\infty \rightarrow b/2} \frac{d\,DW(x)}{dx} \qquad (3)$$

Induced Drag, and Adverse and Proverse Yaw

It is critical to understand the airflow and forces exerted on a wing during flight, including lift and induced drag, to appreciate the differences between the elliptical and bell spanloads, and the implications for birds and aircraft.

Ludwig Prandtl described both the elliptical (1920) and bell (1933) spanload distributions as shown in figure 2. The 1920 elliptical spanload, figure 2(a), describes a wing with a uniform downwash along the wing's trailing edge, and a sharp discontinuity of downwash and upwash at the wingtip, which results in a strong, tightly-rolled vortex formed at the wingtip. In contrast, the bell spanload describes a wing having a downwash that varies from strong downwash near the wing root, which tapers outboard (past b/2 = 0.704), to upwash near the wingtip. The bell spanload is also much more heavily loaded (more net force) in the root area of which the large root downwash is a consequence. The significance of these disparate characteristics is both subtle and dramatic.

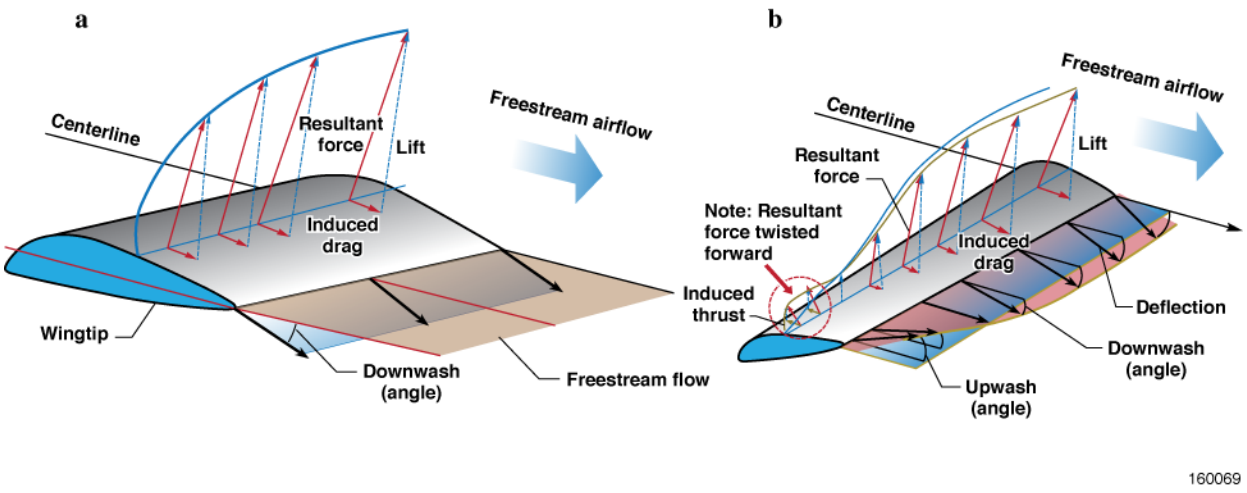

Figure 2. Prandtl's elliptical and bell spanloads explained.

Figure 2(a) shows Prandtl's elliptical spanload from 1920; figure 2(b) the bell spanload from 1933. The symbol gamma (Γ) signifies the airflow circulation about the wing. The matching downwash (dw) of the elliptical spanload and of the bell spanload for each are also shown. The upwash on the 1920 Prandtl elliptical spanload is outboard of the wingtip. Of importance in the elliptical spanload shown in figure 2(a) is that the net force vector field is tilted backwards by the constant downwash along the entire span of the wing. The resulting horizontal component of the resultant force (Γ) manifests itself as induced drag across the entire wingspan. By contrast, in figure 2(b) it can be seen that the 1933 Prandtl bell spanload and downwash show the twisted downwash crossing the zero line and becoming upwash near the wingtip. The resultant force is tilted forward of the vertical and the horizontal component is manifested as induced thrust at the wingtip, due to the resulting upwash.

Airflow over a wing generates a net force, which is approximately normal to the wing chord. As shown in figure 2(a) for an elliptic spanload, this resultant force vector is not exactly perpendicular to the airflow. The larger component perpendicular to the relative wind is known as lift. For finite wings there exists a component parallel to the relative wind (for elliptical spanload, always in the direction with the wind, that is, toward the trailing edge) that is referred to as induced drag. Induced drag is the "cost" of producing lift with a finite wing. As lift increases, induced drag also increases. Thus, any control surface deflected to locally produce more lift will also locally produce more drag. Ailerons deflected anti-symmetrically to generate a rolling moment will also produce a yawing moment to the outside, or against the turn being generated by the roll. This phenomenon is referred to as adverse yaw and is the reason all aircraft with an elliptical spanload require an auxiliary yaw device (typically a rudder, courtesy of the Wright brothers in 1902 [refs. 5, 6]) to counter the adverse yaw in order to coordinate the turn (yaw with the turn).

For the bell spanload, shown in figure 2(b), the net force vector is such that it varies along the span. Inboard, the force vector is tilted away from the relative wind, like that of the elliptical spanload case, and the parallel component produces induced drag. Progressing outboard, this parallel component reduces in magnitude until it eventually (past b/2 = 0.704) is tilted into the relative wind. This phenomenon is referred to as induced thrust (that is, negative induced drag). It should be noted that the sum total force of this parallel component is still producing a net drag (and this sum total is more than that of an elliptical spanload for the same span - in our case we are able to increase the span and achieve less total induced drag), but locally for the outer 0.296 span, it produces thrust. A control surface placed in this local thrust region will generate increasing thrust with increasing lift. Thus an aileron located in this region will produce a yawing moment into the turn, which moment is referred to as a proverse yawing moment. A properly designed aileron, on a bell spanload wing, could produce just the right amount of proverse yaw such that an auxiliary yaw device would be entirely unnecessary for coordinated turning flight. A design without an auxiliary yaw device

means there would be neither added drag nor complexity from such a device. It should be noted that this does not mean for all aircraft designs employing a bell spanload that an auxiliary yaw device would not needed. There are instances on modern aircraft designs (for example, engine-out or crosswind landing) in which such a device would still be needed, but there could be designs for which such a device would not be required. Various bird species appear to maneuver gracefully with very minimal auxiliary yaw devices, and some seemingly have no discernible auxiliary yaw device. Further, as Prandtl pointed out in 1933, it is possible to extend the wingspan of a bell spanload, achieve the same lift and the same integrated wing bending moment, and achieve less induced drag than the equivalent elliptical spanload. This final solution is examined here.

The downwash/upwash curve of the bell spanload is one smooth and continuous function from beyond one wingtip, across the wing to beyond the opposite wingtip. Note that the slope of the downwash/upwash function will also be continuous across the wing. The upwash curve rises from the equilibrium level of the air far beyond the wing tip to a gentle peak at the maximum upwash of the wing, located outboard of the wingtip, which we show as an extension of Prandtl's downwash/upwash. Inboard of the peak, the upwash decreases and meets the upwash of the wing at the wingtip, and the two upwash curves, inboard and outboard, must be of equal slope.

As with any other aircraft, to turn we deflect the control surfaces near the wingtips, increasing the lift near one wingtip, resulting in the desired bank angle. But when we increase the lift on one wingtip the resulting induced thrust also increases (there is always thrust at the wingtips). The raised wing will create more thrust than the lowered wing, resulting in both bank and yaw in the direction of the turn: proverse yaw. As a result of this proverse yaw, coordinated flight is achieved without the need for a tail, rudder, or other drag devices.

Figure 3(a) shows the downwash field behind a wing using the bell spanload through use of twist (Marko Stamenovic). Figure 3(b) shows the vortex roll-up behind the wing, analytical and in flight (Marko Stamenovic and Tom Tschida, NASA photo).

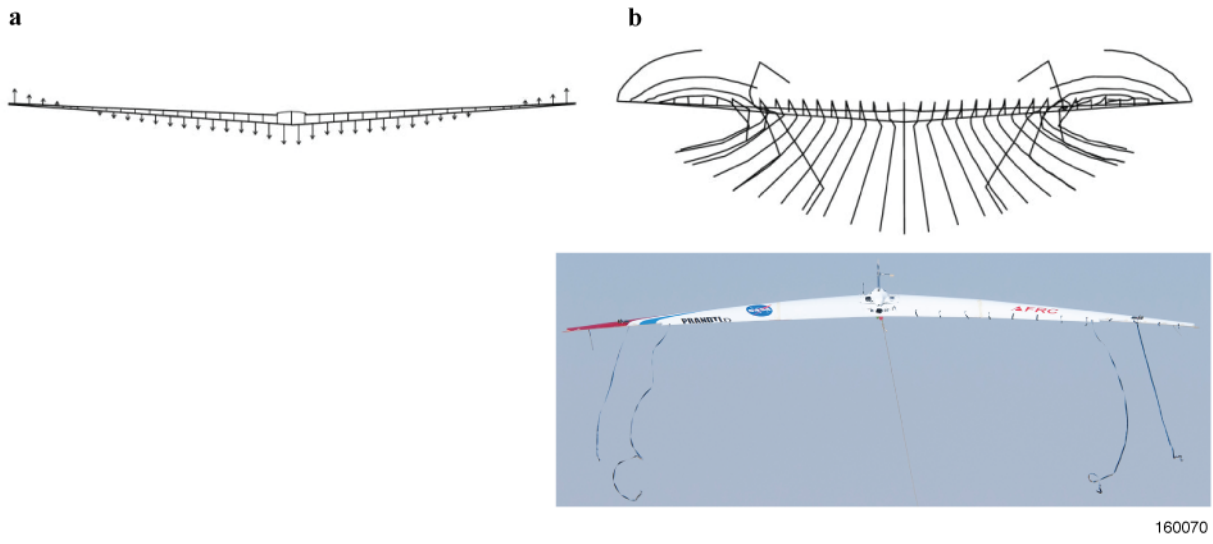

Figure 3. Downwash field, wing vortex roll-up, and resulting wingtip overlap in bird formations.

The Experiment

To validate the theory and the most critical principles of the bell spanload, we conducted an experiment using two subscale flying wing aircraft that used wing twist to achieve the selected bell shaped spanload. The model planform with a bell shaped spanload based on Prandtl's theory was a 25-percent Horten H Xc aircraft (12.3 ft span) with a design lift coefficient of 0.6. The objective of the experiment was to demonstrate coordinated flight with proverse yaw for an aircraft with a bell shaped spanload and no vertical surfaces of any kind on the aircraft. The elevons have equal and opposite throws while functioning as ailerons. There is no differential bias; this is a direct, stick to surface control system.

The Bell Spanload Aircraft Experiment

The radio-controlled aircraft were bungee-launched and flown by a pilot on the ground. Bungee tension was roughly 50 lb at release and typical altitude at separation from the bungee/cord was 200 ft above ground level. The pilot flew the aircraft on a single racetrack pattern during its descent and landing on the dry lakebed from whence it launched, completing various flight dynamics maneuvers en route to collect data. Flight times increased as experience grew, reaching a maximum flight time of 1 min 55 s and averaging nearly 1 min 22 s per flight on aircraft no. 2. Nearly 3 hr of flight time has accumulated.

The first aircraft carried an on-board data collection system: a smartphone with a triad linear accelerometer and triad angular rate recording application. This aircraft also later flew with a microcomputer-based flight data recorder providing basic inertial measurement unit functionality (pitch rate, roll rate, yaw rate, airspeed, and heading). The data sensors included global positioning system, pitot/static system, alpha/beta probes, and control position transducers. Configuration 3 had an open-source data recorder and autopilot, inertial measurement unit, global positioning system, pitot/static system, alpha/beta probes, and control position transducers. All data-gathering and -generating systems were calibrated before flight. Data were downloaded after each flight for later analysis.

Mass Properties

The aircrafts' mass properties are: roll inertia 5.425 slug-ft^2; pitch inertia 0.2717 slug-ft^2 (estimated); yaw inertia 5.818 slug-ft^2; and x-z plane cross product of inertia 0.5054 slug-ft^2. The inertias were measured using a bifilar method, except for pitch inertia, which was estimated from the computer-aided design geometry and the point mass locations of the onboard systems. The center of gravity was placed at 0.128 of the mean aerodynamic chord. The aircraft mass was 14.5 lb. The lateral-directional mass properties proved to be critical to the experiment. Maine and Iliff (ref. 7) show a very high sensitivity to x-z plane cross product of inertia in the estimation of Cnda (yawing moment due to aileron deflection coefficient).

Data Parameters

We gathered flight mechanics data for the aircraft with instrumentation for the following parameters: angle of attack (-20 to 70 deg); angle of sideslip (-45 to 45 deg); total pressure (0 to 2.16 lb/ft^2); static pressure (0 to 2.16 lb/ft^2); normal acceleration (+/-6 g); axial acceleration (+/- 4 g); lateral acceleration (+/- 4 g); roll rate (+/- 200 deg/sec); pitch rate (+/- 200 deg/sec); yaw rate (+/-100 deg/sec); left elevon deflection (+/- 90 deg); and right elevon deflection (+/- 90 deg). The sampling rate was 20 samples per second for all parameters. Open-source microprocessor systems were used for all data collection.

Preliminary Design

We performed preliminary design analyses using two methods: a vortex-lattice model paneling the aircraft as 320 discrete surfaces (ref. 8), each of the discrete surfaces with its own angle; and a build-up of two-dimensional airfoil panel methods (7 span locations, with 5 control surface deflections, 5 chord Reynolds numbers varying from 200,000 to 2,000,000, and at 9 angles of attack from -2 deg to 10 deg). The build-up of the two-dimensional airfoils was integrated in MATLAB (The MathWorks, Inc., Natick, Massachusetts). The airfoils and twist are detailed in Tables 1, 2, and 3. A converged solution was declared between the two result sets when we achieved a four-significant-digit match. The airfoils were custom-designed using the Eppler code (refs. 9, 10). Estimates of the control surface effectiveness were made from the vortex-lattice results and adjusted on the basis of boundary layer thickness. The control surface effectiveness was also adjusted on the basis of the control surface configuration change (plain surface to plain surface with balance added) for the scale of the aircraft. The model scale was set at 25 percent, however, the mass of the vehicle increased due to the addition of the instrumentation package. The resulting wing loading placed the subscale aircraft in the range of the full-scale wing loading; consequently the subscale aircraft flew at velocities closely matching the full-scale aircraft predictions. The wingspan is 12.3 ft with a leading-edge sweep of 24 deg at the nose.

With this in mind for the analysis, the common use of Oswald's efficiency factor ("e") is also not appropriate for bell spanloads. Perhaps the invention of a Prandtl efficiency factor ("p") or a bell efficiency factor ("b") should be used for these Prandtl 1933 bell spanloads. A comparison of the elliptical and bell spanload efficiency parameters is given in table 4.

The coordinate frame for the flight mechanics data on the aircraft is: origin at the center of gravity (12.875 inches aft of the nose); x-axis is positive forward out the nose; y-axis is positive out the right wing; and z-axis is positive down out the bottom of the aircraft. Using a right-hand convention; roll is rotation about the x-axis and is positive for roll right; pitch is rotation about the y-axis and is positive for pitch up; and yaw is rotation about the z-axis and is positive yaw right.

The coordinate frame is: for the wing definition, the x-axis origin is at the wing centerline and extends to b/2 (half-span). The y-axis is defined as vertical upward (though in specific cases it is defined otherwise, and the convention should be apparent by the context).

The aircraft design was generated to produce a bell spanload. The airfoils vary continuously and linearly from the centerline to the tip. The airfoils are specified in nondimensional coordinates. The airfoils used are shown in tables 1 and 2.

Table 1. Airfoil section, centerline.

Wing centerline airfoil							
x	y	x	y	x	y	x	y
0.99839	0.01595	0.33928	0.09971	0.00107	-0.00520	0.40245	-0.01754
0.98664	0.01580	0.30866	0.09846	0.00428	-0.00882	0.43474	-0.01602
0.95215	0.01710	0.27886	0.09632	0.00961	-0.01205	0.46730	-0.01451
0.89696	0.02355	0.25000	0.09339	0.01704	-0.01502	0.50000	-0.01301
0.82387	0.03690	0.22221	0.08978	0.02653	-0.01800	0.53270	-0.01156
0.80438	0.04073	0.19562	0.08553	0.03806	-0.02062	0.56526	-0.01017
0.77779	0.04590	0.17033	0.08072	0.05156	-0.02237	0.59755	-0.00885
0.75000	0.05124	0.14645	0.07539	0.06699	-0.02406	0.62941	-0.00761
0.72114	0.05668	0.12408	0.06963	0.08427	-0.02524	0.66072	-0.00646
0.69134	0.06218	0.10332	0.06345	0.10332	-0.02598	0.69134	-0.00542
0.66072	0.06768	0.08427	0.05691	0.12408	-0.02642	0.72114	-0.00448
0.62941	0.07312	0.06699	0.05017	0.14645	-0.02653	0.75000	-0.00364
0.59755	0.07840	0.05156	0.04318	0.17033	-0.02631	0.77779	-0.00291
0.56526	0.08341	0.03806	0.03575	0.19562	-0.02584	0.80438	-0.00227
0.53270	0.08800	0.02653	0.02897	0.22221	-0.02512	0.82005	-0.00194
0.50000	0.09201	0.01704	0.02201	0.25000	-0.02419	0.89553	0.00255
0.46730	0.09530	0.00961	0.01424	0.27886	-0.02308	0.95184	0.00908
0.43474	0.09777	0.00428	0.00784	0.30866	-0.02184	0.98662	0.01411
0.40245	0.09936	0.00107	0.00353	0.33928	-0.02047	0.99839	0.01595
0.37059	0.10000	0.00000	0.00000	0.37059	-0.01904		

Table 2. Airfoil section, wingtip.

Wingtip airfoil							
x	y	x	y	x	y	x	y
1.00000	0.00070	0.40620	0.04556	0.00002	-0.00038	0.46904	-0.04274
0.96091	0.00428	0.38108	0.04644	0.00028	-0.00161	0.48162	-0.04208
0.94833	0.00540	0.36853	0.04682	0.00174	-0.00435	0.49420	-0.04139
0.93571	0.00654	0.35599	0.04716	0.00460	-0.00763	0.50678	-0.04067
0.92307	0.00769	0.34346	0.04745	0.00681	-0.00956	0.54455	-0.03836
0.89778	0.00999	0.33093	0.04770	0.01384	-0.01430	0.55715	-0.03754
0.88515	0.01114	0.29342	0.04814	0.01925	-0.01718	0.56975	-0.03670
0.84728	0.01455	0.26848	0.04816	0.02619	-0.02030	0.59495	-0.03496
0.82206	0.01679	0.25604	0.04807	0.03452	-0.02347	0.60756	-0.03406
0.80944	0.01789	0.24362	0.04791	0.06460	-0.03186	0.62017	-0.03315
0.79683	0.01898	0.23122	0.04767	0.07556	-0.03415	0.65801	-0.03031
0.78422	0.02006	0.21885	0.04736	0.09825	-0.03801	0.67063	-0.02933
0.77160	0.02113	0.20652	0.04696	0.12166	-0.04103	0.68325	-0.02834
0.73374	0.02428	0.15762	0.04434	0.13355	-0.04229	0.69587	-0.02734
0.72112	0.02531	0.14554	0.04338	0.14554	-0.04338	0.72112	-0.02531
0.69587	0.02734	0.13355	0.04229	0.15762	-0.04434	0.73374	-0.02428
0.68325	0.02834	0.12166	0.04103	0.20652	-0.04696	0.77160	-0.02113
0.67063	0.02933	0.09825	0.03801	0.21885	-0.04736	0.78422	-0.02006
0.65801	0.03031	0.07556	0.03415	0.23122	-0.04767	0.79683	-0.01898
0.62017	0.03315	0.06460	0.03186	0.24362	-0.04791	0.80944	-0.01789
0.60756	0.03406	0.03452	0.02347	0.25604	-0.04807	0.82206	-0.01679
0.59495	0.03496	0.02619	0.02030	0.26848	-0.04816	0.84728	-0.01455
0.56975	0.03670	0.01925	0.01718	0.29342	-0.04814	0.88515	-0.01114
0.55715	0.03754	0.01384	0.01430	0.33093	-0.04770	0.89778	-0.00999
0.54455	0.03836	0.00681	0.00956	0.34346	-0.04745	0.92307	-0.00769
0.50678	0.04067	0.00460	0.00763	0.35599	-0.04716	0.93571	-0.00654
0.49420	0.04139	0.00174	0.00435	0.36853	-0.04682	0.94833	-0.00540
0.48162	0.04208	0.00028	0.00161	0.38108	-0.04644	0.96091	-0.00428
0.46904	0.04274	0.00002	0.00038	0.40620	-0.04556	1.00000	0.00070
0.43132	0.04453	0.00000	0.00000	0.43132	-0.04453		

The wing twist is nonlinear; it is specified at 20 intervals from the centerline to the wingtip, in degrees, as shown in table 3. Using the above airfoil coordinates, this twist does not require any compensation for aerodynamic twist relative to the geometric twist.

Table 3. Wing twist distribution.

Wing twist			
0	8.3274	11	7.2592
1	8.5524	12	6.6634
2	8.7259	13	5.9579
3	8.8441	14	5.1362
4	8.9030	15	4.1927
5	8.8984	16	3.1253
6	8.8257	17	1.9394
7	8.6801	18	0.6589
8	8.4565	19	-0.6417
9	8.1492	20	-1.6726
10	7.7522		

The control surfaces are located in the outboard 14 percent of each wing, in the trailing 25 percent of the chord; the round tips are included as part of the control surfaces. The wingspan is 12.3 ft, the wing area is 10.125 ft^2, the centerline chord is 15.75 in., and the wingtip chord is 3.94 in. The wing had 2.5 deg of dihedral.

Table 4. Elliptical spanload and bell spanload comparison of spanload parameters and efficiency factors.

Spanload parameter	Elliptical spanload	Bell spanload
b/2	1.0000	1.2247
Cdi	1.0000	0.8889
e	1.0000	0.8889

This comparison is made using the traditional elliptical spanload as the baseline from which the bell spanload is compared.

In figure 4, three spanloads (blue = -5 deg; red = 0 deg; and green = +5 deg) are plotted showing the effect of sideslip on the area of induced thrust near the wingtips and the resulting effect on yawing moment. The light-green line shows a large area of induced thrust on the left and a small area of induced thrust on the right, which would result in a large right-yawing moment.

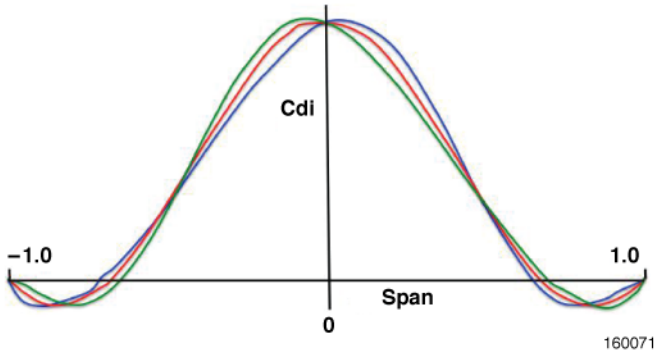

Figure 4. Effect of sideslip on bell spanload with twist (0 and +/- 5 deg).

Aerodynamic Coefficient Estimation

We used Maine and Iliff's output-error approach to estimate the aerodynamic coefficients, which was the same source used for the estimates of Cnda. We assume the aircraft is a continuous-time dynamic system. The process of estimating the aerodynamic coefficients is an exercise in system identification. Assumptions were made in this process, many based on previous experience, such as which parameters were important (these are retained) and which were not (these are ignored). This approach uses a formulation of the solid-body aircraft flight mechanics as a linear simulation of the vehicle. An initial estimate is made of the aerodynamic coefficients; the simulation then makes an estimate of the vehicle motion based on the aerodynamic coefficients, the mass properties, and the equations of motion, after which the linear estimates are compared to the measured flight data from the vehicle. Errors from all of these measurements subject the final estimates of the aerodynamic coefficients to uncertainty. The errors between the simulation output and the measured data are subjected to a measurement based on a weighted error-based cost function defined by the researchers.

The aerodynamic coefficient estimates are then varied, and slopes or gradients are determined numerically from the errors. The estimation program then marches toward minimizing the cost function from the "fit" between the output of the linear simulation and the measured flight data. Maneuvers were simple doublet maneuvers, which are simple square-wave pulses, both positive, followed immediately by a similar pulse of the opposite sign.

The results of the flight research on the small flying wing glider were successful, as can be seen in figure 5(a). We measured proverse yaw in flight for the first time on June 27, 2013. A sample output from the flights shows proverse yaw, as shown in figure 5(b).

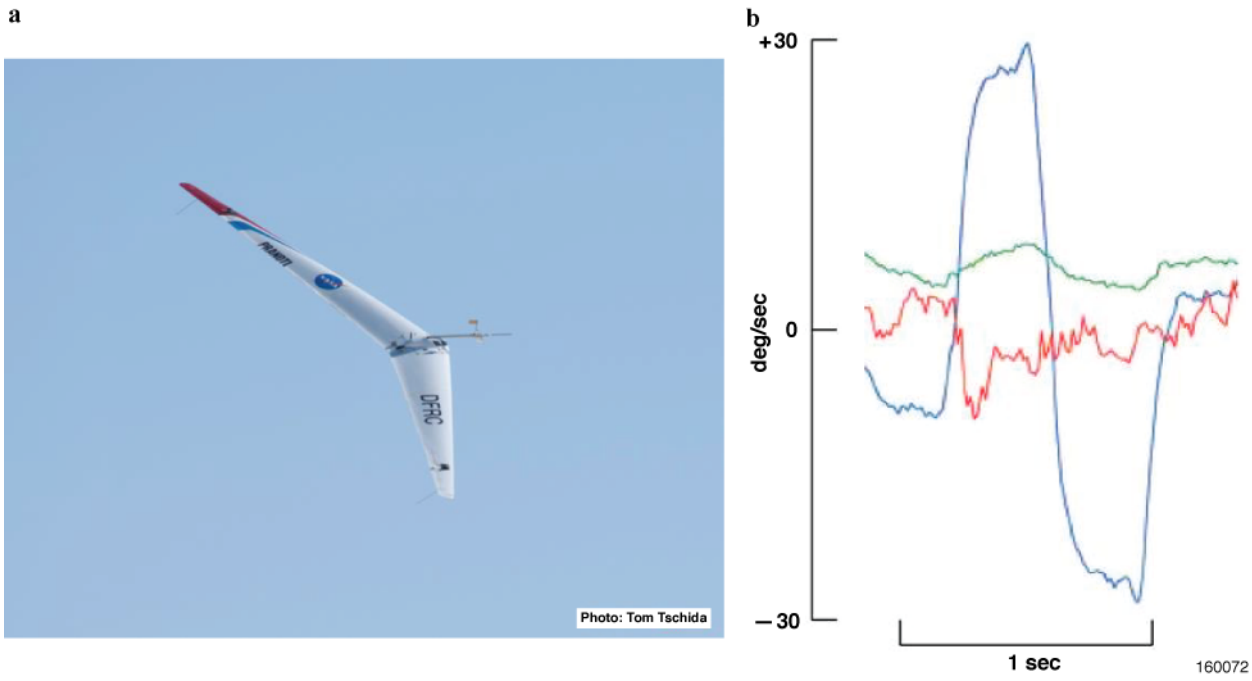

Figure 5. A subscale aircraft in flight, and resulting proverse yaw data trace.

Figure 5(b) shows a data trace of the angular rates from onboard instrumentation. Red is pitch rate, blue is roll rate, and green is yaw rate. The high-frequency motion in pitch rate is due to air turbulence. The yaw motion following the roll motion is the same sign; the yaw gain is 0.0643 and correlation is 0.77 for this maneuver. All rates are to the same scale.

We calculated the coefficient Cnda from the flight research maneuvers. In figure 6, the scattered dots represent the flight research maneuvers. The value of Cnda is positive and the trend of the slope is also positive. The degree of scatter in the data is a result of all experimental error. From this we see that Cnda is providing the yawing moment in the same direction as the rolling moment.

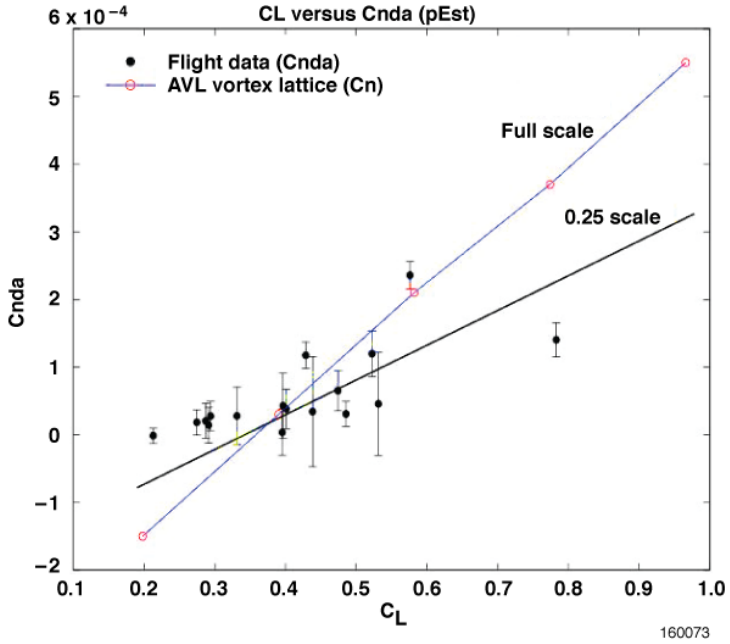

Figure 6. Yawing moment due to aileron deflection coefficient versus lift coefficient.

The yawing moment due to aileron deflection coefficient (Cnda) is shown plotted against lift coefficient in figure 6. The blue line and red circles were predicted for the full-scale aircraft. The black line is an estimate of the 0.25-scale experiment aircraft. The black dots are the estimates from flight data. Error bars are 5x Cramer-Rao bounds. The straight line with the circles represents the analytical data from the vortex lattice. An estimate of the effect of scale is made on the vortex-lattice (reducing the scale reduces the effectiveness of the control deflection and reduces the resulting yawing moment). The good comparison between the predicted and the measured flight Cnda confirmed our expectations regarding Prandtl's bell spanload.

Birds and the Bell Spanload

There are at least two larger implications of this work. The first is for the avian research community; the second is for the aeronautical world.

That birds have no vertical tail yet effect effortless turns remains a puzzle, inasmuch as all avian flight research is analyzed using the elliptical spanload. The matter of formation flight also defies satisfactory explanation despite a century's worth of research, analysis and effort, again in large part because the analysis relies entirely on the elliptical spanload. ("The wake [of the kestrel] was found to be similar to that measured behind an elliptically loaded airfoil of the same span," wrote Geoff Spedding when analyzing his data. "As a result, classical airfoil theory for an elliptically loaded wing was used to calculate parameters such as lift coefficients and efficiency factors" (ref. 11). Less apparent but equally puzzling to close observers is the shape of birds' wings when compared to aircraft wings: the former taper, often to a sharp point, while the latter rarely do, and this, too, defies the elliptical spanload solution. The load distribution over a bird's wing is far more gradual than an elliptical spanload provides: consider a birds' wing

structure—both skeletal and on the surface—which tapers to almost nothing near the tips, where the outermost feathers carry virtually no load at all, as compared to an aircraft's wing. An elliptically loaded aircraft's wings carry loads right to the wingtip.

First, based on our research results we assert that the growing data on bird flight is irreconcilable so long as it relies on the elliptical spanload as the analytical tool. Second, based on the analytical results of the bell spanload and the flight data, we assert the only viable solution for interpreting bird flight, formation flight, and bird wing structure is the bell spanload.

We know that it is a biological imperative that birds carry no excess structure in their wings or chest muscles, only as much as muscle, tendon, and bone as necessary. Birds embody minimum structure while achieving maximum aerodynamic efficiency while accomplishing coordinated flight: birds are a solution to a multivariate optimization. Recall that Prandtl's second paper provided a spanload solution to maximum efficiency for a given structural weight when the wingspan need not be constrained. The bell spanload is the only explanation for how birds achieve this multivariate solution (refs. 12-15).

Birds-Bell Spanload; Airplanes-Elliptical Spanload

1. Birds' primary feathers are soft and flexible at their wingtips and the wings have a narrow chord; these wingtip feathers are incapable of supporting any substantial load. Additionally, the outboard wing structures of birds are long and slender. The ligaments, tendons, supporting muscles, and bones are long and thin, improving aerodynamic performance, but the load-carrying ability of these structures is very modest (the same was true for pterosaurs). In contrast, aircraft wingtip structures are large, heavy, and expected to carry real loads in flight.

2. Birds flying in formation position themselves to capture upwash from a leading bird's wing vortex roll-up for added efficiency. Data shows they do this with wings overlapped. Aircraft flying in formation with similar objectives do not match this profile, however: they fly with wingtips in line.

3. Birds do not experience wingtip stall even with their narrow-chord, sharp-tipped, wings. But when sharp-tipped swept wings are used on aircraft, wingtip stall is common and requires other solutions to overcome.

We are accustomed to seeing birds turn and maneuver without a vertical tail, and only seeing aircraft do so using such drag-inducing devices. The ability to turn and maneuver without resorting to drag-inducing devices to counter adverse yawing forces is the first evidence for why the bell spanload—which generates proverse yaw—explains the flight of birds.

Figure 7 shows a wandering albatross (diomedea exulans) in flight. The wandering albatross has no vertical tail, yet these birds are able to expertly fly so that they precisely touch their wingtips to the water.

Figure 7. Wandering albatross in flight.

Researchers such as Wieselsberger (ref. 16), Lissaman and Schollenberger (ref. 17), and Portugal have argued that flying in formation allows birds to capture upwash in the air from the wing vortex roll-up. There is no dispute that birds maximize the energy from the upwash, something only possible in formation flight. What we dispute is where that vortex occurs on birds. Figure 8(a) shows a formation of pelicans flying with wingtips overlapped, which is an optimal arrangement with the bell spanload but suboptimal for the elliptical spanload because in this case the vortex roll-up is not at the wingtip but inboard of the wingtip (at .704 of the semi-span) and is in fact a wing vortex roll-up, not a wingtip vortex roll-up. Spedding's data support this, as can be seen in figure 8(b); the vortices seen behind his kestrel show a vortex roll-up inboard of the wingtips. ("This wing loading distribution [elliptical] is reflected in the geometry of the wake," he wrote). Birds position themselves in formation flight based on the location of the actual vortex roll-up, and only the bell spanload generates a vortex roll-up in that location.

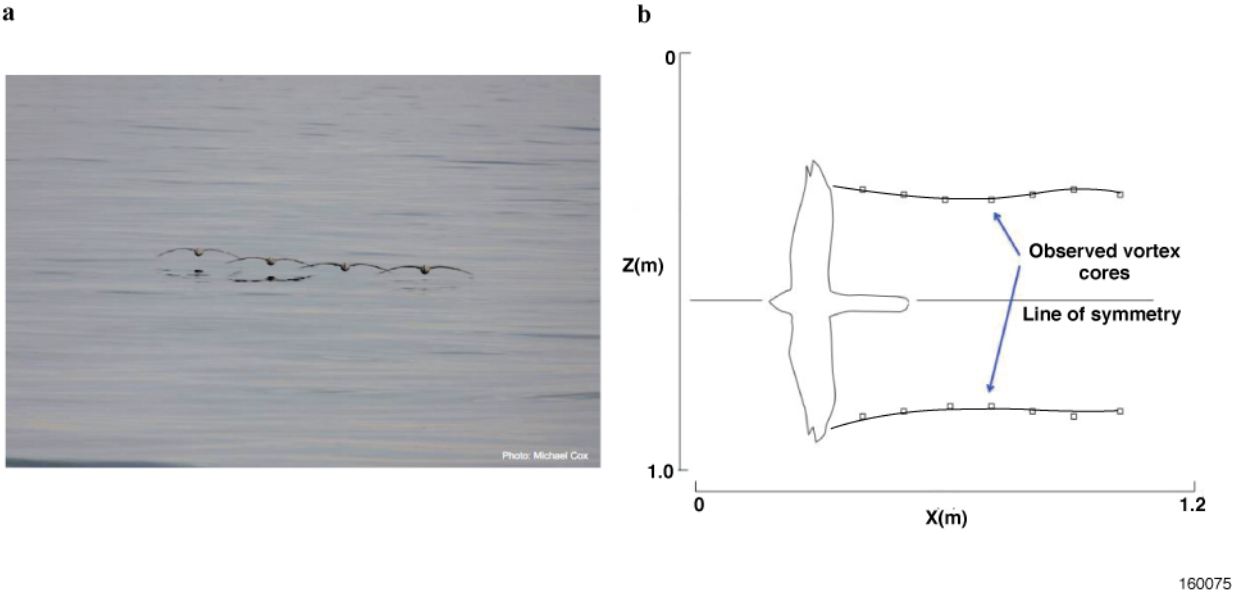

Figure 8. Significant bird flight characteristics; a: Formation flight of brown pelicans (pelecanus occidentalis) demonstrating the resulting wingtip overlap; and b: Spedding's kestrel (falco tinnunculus) data showing an inboard vortex core location.

Figure 9(a) shows spanwise location data of following bird relative to the lead bird in the northern ibis (geronticus eremita) from Portugal, with Hainsworth (ref. 18), Cutts & Speakman (ref. 19), and Speakman & Banks (ref. 20). Figure 9(b) shows an overlay of the data sets with our addition of the downwash curve of the Prandtl 1933 spanload and our extension of Prandtl's 1933 theorum.

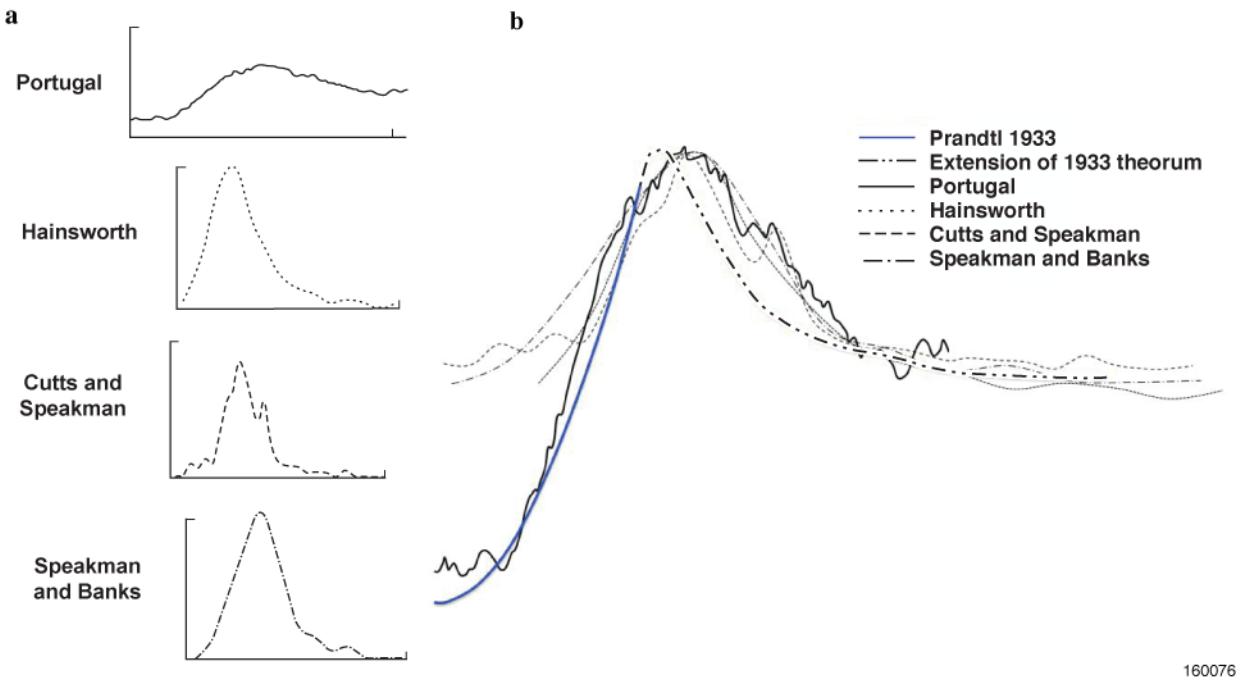

Figure 9. Bird position in formation flight.

Portugal recently published research based on global positioning system data showing northern ibis flying in formation with the tips of their wings overlapping. He concluded that the mean spacing was 0.904 m on a mean wingspan of 1.2 m, for a vortex core separation of 0.753. Spedding gave the vortex core separation of his kestrel research as 0.76 of span. The vortex separation on our research flying wing aircraft occurred at 0.704 of the semispan. Portugal, like Spedding and others before him, analyzed his results using the elliptical spanload, forcing the analysis of the birds to fly formation with their wingtips in line with each other rather than with wings overlapped. Birds in formation flight seek out the greatest upwash, and there is a clear, strong correlation between the location data of birds in formation flight and the vortex formation and upwash data of the bell spanload.

How are birds able to fly with pointed wingtips? Note how the lift tapers gradually to zero at the wingtip with the bell spanload. The result is that even wings with very strongly tapered tips show no tendency to wingtip stall. Rather than occurring at the wingtip (as it will with an elliptical spanload) the stall begins about 20 percent out from the wing root, something observable in the flight of birds [figure 10(b)]. Because the bell spanload creates proverse yaw in the outer third of the wing, the thrust yields controllability even with a sharply tapered wing.

The upwash at the tips of the bell spanload makes it possible to capture the wingtip-induced thrust that can then generate coordinated roll and yaw without resorting to the use of a vertical tail and without generating drag at the wingtips. If we accept Prandtl's 1933 lift distribution as useful for birds, it follows that birds are manipulating thrust at their wingtips to control yaw.

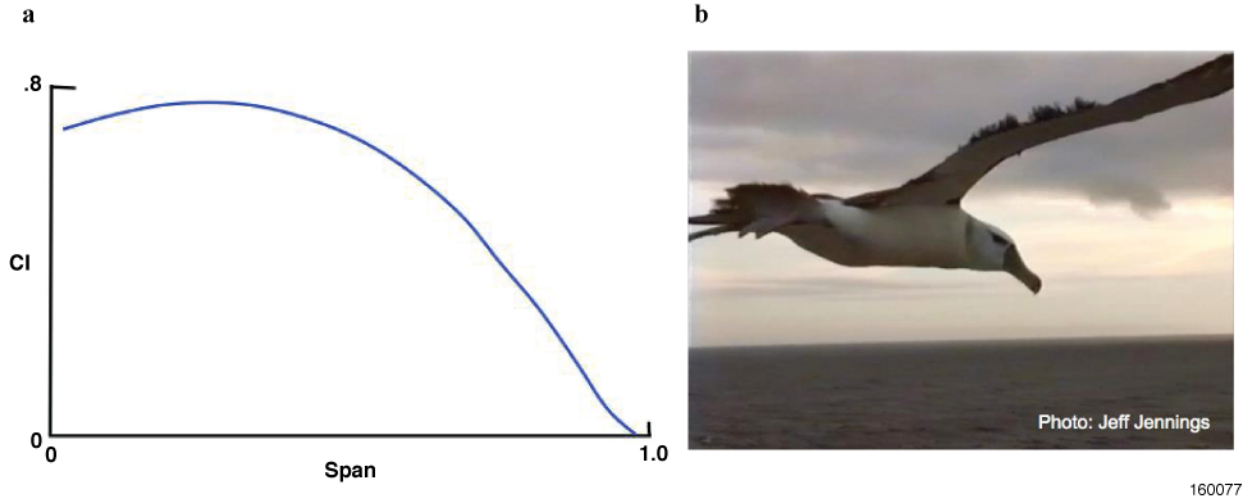

Figure 10. The local lift coefficient (Cl) and the beginning of stall on the wing of a wandering albatross.

Figure 10(a) shows the local lift coefficient as a function of span for a bell spanload from centerline to the wingtip. Note that the highest point on the curve is the area in which the wing would first stall. Figure 10(b) shows an image of a wandering albatross soaring at low speeds (image by Jeff Jennings). Ruffled feathers indicate the beginnings of the stall, at approximately 20 percent of span, not near the tip, matching the bell spanload predictions.

Combining observational evidence and data developed by avian researchers with our own research results, we assert that only the bell spanload provides a coherent paradigm for bird flight. Our research offers for the first time a theory and a tool derived from flight test that satisfactorily explains bird flight to match the data. It also serves as a solution to far more efficient aircraft flight.

Conclusion

The bell spanload maximizes aerodynamic efficiency with a given structure, coordinates the roll-yaw motion so that birds are able to turn and maneuver without a vertical tail, and explains why birds fly in formations with their wingtips overlapped, as well as how birds use narrow wingtips without experiencing tip stall.

The bell spanload also allows for improved aircraft designs, particularly all flying-wing aircraft and blended-wing body aircraft. Even conventional tailed aircraft can benefit from the improved aerodynamics and minimum structure approach. There are circumstances in which span constraints exist (such as extremely large transport category aircraft), in which cases current approaches provide better solutions.

Neither Prandtl nor Horten followed through to the logical and complete conclusion of their work. Prandtl did not extend the upwash outboard of the wingtip, which would have answered the question of formation flight in birds, and he did not find the induced thrust at the outboard ends of the wings, which leads to proverse yaw. In turn, with his approximation and objectives Horten did not understand the origin of the induced thrust at the outboard ends of the wings for proverse yaw, and he did not prove that proverse yaw exists.

It remained for the current authors to prove conclusively that proverse yaw is achievable through an efficient bell-shaped spanload, that an optimal solution integrating minimum structure and minimum drag can solve the problem of yaw control and stability of a flying wing, and that the bell spanload solution answers some of the great enduring mysteries of the flight of birds.

In the case of the flight of birds, the bell spanload is the only viable solution.

References

1. Prandtl L (1921) Applications of modern hydrodynamics to aeronautics, NACA Report No 116 (Washington, DC).

2. Prandtl L (1933) Über tragflügel kleinsten induzierten widerstandes. Zeitschrift für Flugtecknik und Motorluftschiffahrt, 1 VI 1933 (München, Deustchland).

3. Horten R, Selinger P with Scott J (translator) (1985) Nurflugel: The story of Horten flying wings 1933 – 1960. Weishapt Verlag, Graz, Austria.

4. Lee R (2011) Only the wing: Reimar Horten's epic quest to stabilize and control the all-wing aircraft. Smithsonian Institution Scholarly Press, Washington D.C. 312 p.

5. McFarland M (1953) The papers of Wilbur and Orville Wright including the Chanute-Wright letters and other papers of Octave Chanute, vols. 1 and 2.

6. US Patent and Trademark Office (1906) O. & W. Wright, Flying Machine. Patent Number 821,393.

7. Maine RE, Iliff KW (1986) Application of parameter estimation to aircraft stability and control - the output-error approach. NASA RP-1168.

8. Margason RJ, Lamar JE (1971) Vortex-lattice FORTRAN program for estimating subsonic aerodynamic characteristics of complex planforms. NASA TN D-6142.

9. Eppler R, Somers DM (1980) A computer program for the design and analysis of low-speed airfoils. NASA TM-80210.

10. Bowers AH, Sim AG (1984) A comparison of Wortmann airfoil computer-generated lift and drag polars with flight and wind tunnel results. NASA TM-86035.

11. Spedding GR (1987) The wake of a kestrel (falco tinnunculus) in gliding flight. J. Exp. Biol.,127, 45-57.

12. Humphries NE, Weimerskirch H, Queiroz N, Southall EJ, Sims DW (2012) Foraging success of biological Lévy flights recorded in situ. DOI: 10.1073/pnas.1121201109.

13. Sachs G, et al. (2012) Flying at no mechanical energy cost: disclosing the secret of wandering albatrosses. DOI: 10.1371/journal/pone.0041449.

14. Weimerskirch H, et al. (2013) Changes in wind pattern alter albatross distribution and life-history traits. DOI: 10.1126/science.1210270.

15. Portugal SJ et al. (2014) Upwash exploitation and downwash avoidance by flap phasing in ibis formation flight. DOI: 10.1038/nature12939.

16. Wieselsberger C (1914) Beitrag zur Erklärung des Winkelfluges einiger Zugvögel. Zeitschrift für Flugtechnik und Motorluftschiffahrt, 15 VIII 1914 (München, Deustchland).

17. Lissaman PBS, Shollenberger, CA (1970) Formation flight of birds. DOI: 10.1126/science.168.3934.1003.

18. Hainsworth FR (1988) Induced drag savings from ground effect and formation flight in brown pelicans. J. Exp. Biol. 135, 431-444.

19. Cutts CJ, Speakman JR (1994) Energy savings in formation flight of pink footed geese. J. Exp. Biol. 189, 251-261.

20. Speakman JR, Banks D (1998) The function of formations in Greylag geese anser anser; energy saving or orientation? Ibis 140, 280-287.